

# Corrosion of Cold Spray Deposited Copper Coating on Steel Substrates

Raheleh Partovi-Nia,\* Sridhar Ramamurthy,†\*\* Dmitriy Zagidulin,\* Jian Chen,\* Rebecca Jacklin,\*\* Peter Keech,\*\* and David W. Shoesmith\*\*\*

## ABSTRACT

The corrosion behavior of copper cold spray coatings on a carbon steel substrate was compared to that of commercially available wrought copper under the conditions anticipated in a nuclear waste repository. Corrosion potential and linear polarization resistance measurements were conducted over 90 d to 120 d in 3.0 mol/L NaCl under anoxic (1) and oxygenated-to-anoxic (2) conditions to simulate the long (1) and short (2) term redox conditions expected in a Canadian repository. Scanning electron microscopy and x-ray diffractometry were used to observe the morphology of the corroded surface and to identify the corrosion products formed. The two specimens behaved very similarly under both sets of conditions. Negligible corrosion was observed under anoxic conditions and the formation of both  $\text{Cu}^{+1}$  ( $\text{Cu}_2\text{O}$ ) and  $\text{Cu}^{+2}$  ( $\text{Cu}_2(\text{OH})_3\text{Cl}$ ) phases occurred under oxygenated conditions. No evidence was observed to suggest the particle boundaries in the cold sprayed coating were preferential corrosion sites.

**KEY WORDS:** cold spray coating, copper, corrosion, underground disposal, used fuel container

## INTRODUCTION

The recommended approach for the long-term management of nuclear fuel waste in Canada is Adaptive

Phased Management.<sup>1</sup> This approach includes the possibility of centralized containment and the isolation of the used fuel in a deep geologic repository in a suitable rock formation. The Canadian repository concept is based on multiple barriers: the used fuel bundles, a durable metal container, a clay buffer and seals around the container, and a deep geologic environment.<sup>2</sup> A key barrier in this sequence is the container. Various container designs have been considered internationally,<sup>3-6</sup> and one possible Canadian design would be fabricated with a carbon steel vessel and an outer shell of ~25 mm-thick copper (Cu). The inner steel (100 mm thick) vessel would provide structural support and containment, while the outer Cu shell would act as a corrosion barrier.<sup>7</sup> This container, and the surrounding bentonite clay, would be exposed to either moderately saline groundwater in crystalline rock or to highly saline groundwater in sedimentary rock in the deep geologic repository. It has been estimated that Cu corrosion on such a container would be less than 1.27 mm over 1 million y, during which the used fuel would be isolated within the container.<sup>8</sup>

While such a used fuel container is technically feasible,<sup>4</sup> there are significant manufacturing challenges associated with this design and the commercial production of large numbers of containers. The need for a narrow gap (~1 mm) between the steel vessel and the Cu shell is a difficult challenge because it must be maintained over a container length of 4 m. In addition, Cu tube shells (i.e., with a thickness less than ~50 mm and a large radius and length) cannot be manufactured by conventional means (i.e., extrusion, pierce-drawing) because of the inherent flexibility of

Submitted for publication: May 1, 2015. Revised and accepted: July 12, 2015. Preprint available online: July 12, 2015, <http://dx.doi.org/10.5006/1757>.

† Corresponding author. E-mail: [sramamur@uwo.ca](mailto:sramamur@uwo.ca).

\* Department of Chemistry, University of Western Ontario, 1151 Richmond Street, London, N6A 5B7, Canada.

\*\* Surface Science Western, Western University, 999 Collip Circle, London, N6G 0J3, Canada.

\*\*\* Nuclear Waste Management Organization, 22 St Clair Avenue East, Toronto, M4T 2S3, Canada.

**TABLE 1**  
Composition of Materials Used in this Study

Material	Composition																			
	wt%			ppm																
	Cu	O	H	Ni	Fe	Ag	S	P	Sn	Zn	Te	Pb	Se	Mn	Sb	Bi	Cd	As	Pd	P
Cu powder used for cold spray copper coating	99.76	0.2	0.002	103	61	<13	10	<3	<2.1	1.4	<1	<1	<1	0.9	0.6	<0.3	<0.1	<0.1		
WCu	Bal.	0.0005		10	10	25	15		2	1	5		3	0.5	4	1	1	5	5	3
pWCu	Bal.	0.0003	0.0004	1	2	13	10	30-100	0.3	0.3	1	1	1	0.1	0.3	0.2	0.1	<0.1		

pure Cu,<sup>8-11</sup> which would lead to distortions during handling/cooling. The consequences of incorrectly machining components of a dual-walled container are also potentially severe, as a gap of a few mm between the steel and copper could cause a creep rupture.<sup>12</sup> In addition, there is an ongoing debate regarding creep measurements and the fundamental understanding of the mechanisms used to make predictions that can be applied to very long time periods.<sup>13</sup>

To overcome these challenges, the Canadian Nuclear Waste Management Organization has initiated an extensive program<sup>14</sup> to design and develop Cu corrosion barriers as coatings or claddings formed directly on the surface of the steel vessel. Cold spray is one coating method being investigated. The cold spray technique uses high-pressure and high-temperature gas to drive fine Cu powder onto the substrate with sufficient kinetic energy to produce a strong mechanical bond, forming a coating without exceeding the powder melting temperature. The advantages of this technique are that the coating layer is rigid and free from oxidation with an easily controlled thickness.<sup>14-16</sup>

In the current study, Cu-coated samples were prepared using this cold spray coating technique, and their corrosion properties were compared to those of wrought Cu for which a substantial corrosion database already exists. The primary goal of this study was twofold: (i) to determine whether the presently available corrosion database for Cu is applicable to these coatings, and (ii) to elucidate those features of the fabrication process which may influence the morphology and distribution of corrosion damage.

## EXPERIMENTAL PROCEDURES

### Sample Preparation

Cold spray specimens were produced by the Surface Technologies Group (Advanced Forming and Coatings Division) at the Industrial Materials Institute

of the National Research Council (NRC) of Canada, Quebec. The specimens were fabricated using low oxygen (O) content commercial Cu powder to deposit the coatings on 12.5 cm × 15 cm mild steel substrates. The composition of the Cu particles, determined by NRC in accordance with the methods referenced in ASTM B152,<sup>17</sup> is presented in Table 1. The particles were spherical, with a size ranging from a few micrometers to 30 μm, with a mean size of 13.1 μm. Cold spray deposition was performed using either He gas, or a sequence of He followed by N<sub>2</sub> gas, at 800°C to maximize particle velocity and avoid O uptake. On completion of the cold spray process, small cylindrical specimens (~8.85 mm in height and 15 mm in diameter) were cut from the coated plate using an electric discharge machine. The Cu coating was ~2.5 mm thick. The coatings formed using only He (as-deposited cold spray [ADCS]) were used in the as-received condition, while those formed using He followed by N<sub>2</sub> (cold spray annealed [CSA]) were first annealed (350°C for 1 h) and then polished as described later. Wrought polycrystalline C10100 Cu (designated WCu, UNS C10100)<sup>(1)</sup> in the as-received condition and SKB<sup>†</sup> Cu in the polished condition (to a 0.25 μm diamond paste, designated pWCu) were used to provide a basis for comparison to the coated specimens. pWCu, a P-doped oxygen-free Cu, was supplied by the Swedish Nuclear Fuel and Waste Management Company. Compositions of WCu and pWCu are also presented in Table 1.

All specimens used in the corrosion experiments were mounted face down (exposing a single Cu surface) in Loctite Hysol<sup>†</sup> epoxy resin, which is a two-part epoxy system with a resin and a hardener. After mounting, the epoxy resin was cured at room temperature for 24 h. Polished specimens were ground using wet SiC papers successively from P80 to P4000 grit and finally polished sequentially to a 3, 1, and 0.25 μm diamond finish using Varsol<sup>†</sup>.<sup>18</sup>

### Experimental Methodology

Specimens were examined using either a Zeiss Axioplan Compound Microscope<sup>†</sup> or Discovery V8

<sup>(1)</sup> UNS numbers are listed in *Metals and Alloys in the Unified Numbering System*, published by the Society of Automotive Engineers (SAE International) and cosponsored by ASTM International.

<sup>†</sup> Trade name.

Stereomicroscope<sup>†</sup>, and the coating surface morphology and composition were determined using either a Hitachi S-4500<sup>†</sup> field emission scanning electron microscope or a LEO 440<sup>†</sup> scanning electron microscope (SEM), both equipped with a Quartz XOne<sup>†</sup> energy dispersive x-ray analysis (EDX) system. SEM/EDX analyses were performed using a 15 keV beam voltage. X-ray diffraction (XRD) was performed with a Bruker D8<sup>†</sup> fully automated diffractometer using CuK $\alpha$  radiation ( $\lambda = 1.78897 \text{ \AA} = 0.178897 \text{ nm}$ ). The XRD patterns were fitted with X'pert High Score Plus<sup>†</sup> (version 1.0d).

Electrochemical measurements were performed using a standard three-electrode electrochemical cell. The resin-sealed specimens were used as the working electrode, and a saturated calomel electrode (SCE,  $0.242 V_{\text{SHE}}$ ) and Pt foil were used as the reference and counter electrodes, respectively. Corrosion potential ( $E_{\text{corr}}$ ) and polarization resistance ( $R_p$ ) measurements were performed using a Solartron 1287<sup>†</sup> potentiostat and the Corrware/CorrView<sup>†</sup> software (version 3.3e).  $R_p$  measurements were performed using the linear polarization resistance (LPR) technique by scanning the potential  $\pm 10 \text{ mV}$  from  $E_{\text{corr}}$  at a scan rate of  $10 \text{ mV/min}$ , and required a total of 4 min.  $R_p$  values were defined as the linear averaged slope of the voltage/current density relationship. Experiments were conducted in a 3 mol/L NaCl solution sparged with either high purity  $O_2$  or Ar gas depending on the redox conditions required. The solutions were prepared using reagent grade chemicals and Type I water (as per ASTM Standard D1193-06<sup>19</sup>).

Experiments were conducted under two distinct redox conditions. One set was performed in an anaerobic chamber to achieve the anoxic conditions anticipated in a waste repository at long times. In a second set of experiments, the solution was  $O_2$ -saturated for the first 24 d and then degassed by Ar-sparging for the remainder of the experiment. This second experiment attempted to simulate the anticipated evolution in repository conditions from initially oxidizing to eventually anoxic,<sup>4</sup> although the duration of the experiment did not reproduce the extended period anticipated for such a change in the redox environment under repository conditions. For experiments conducted in the anaerobic chamber, the Cu specimens were placed in the main chamber through a purged introduction chamber. Type I  $H_2O$  and NaCl salt were also introduced to the main chamber using the same procedure. Type I  $H_2O$  was kept in the chamber for  $> 20 \text{ h}$  to achieve equilibrium with the atmosphere within the chamber. The 3.0 mol/L NaCl solution was prepared inside the chamber after this equilibration period, and experiments commenced after waiting for 1 h.

The minimum measurable  $[O_2]$ , set by the detection limit of the  $O_2$  sensor in the anaerobic chamber, was 1 vppm. The actual vapor phase ( $O_2 + H_2O$ ) con-

centration may have been considerably less than 1 ppm. Using Henry's Law, a value of  $10^{-6} \text{ atm}$  ( $101.325 \times 10^{-6} \text{ kPa}$ ) for the partial pressure of  $O_2$  in the chamber (the total chamber pressure being 1 atm [ $101.325 \text{ kPa}$ ]), and a Henry's law constant of  $769.2 \text{ L}\cdot\text{atm/mol}$  ( $7.79 \times 10^4 \text{ L}\cdot\text{kPa/mol}$ ) for  $O_2$  at 298 K, the dissolved  $[O_2]$  was estimated to be  $\leq 0.042 \text{ ppb}$ .<sup>20</sup>

## RESULTS

### Characterization of Cold Spray Copper-Coated Steel Samples

A number of optical microscopy and SEM studies have been conducted to characterize both the deformed particles used in the spray and the as-sprayed coatings and the results from these measurements are presented elsewhere.<sup>21-23</sup> These studies show the coatings are relatively dense, with a low porosity (observed by SEM on as-received specimens and polished cross sections) and that the interparticle boundaries are generally observable. By comparison, the wrought Cu is nearly defect free, with no visible pores.<sup>24</sup>

Figure 1 shows SEM images for the four surfaces. The surface of the ADCS specimen was extensively deformed, with the boundaries between the particles clearly delineated. The concave surface features indicated that some impinging particles damaged the surface without adhering. After grinding and polishing, the surface of the annealed (CSA) specimen was generally smooth but retained some small voids. By comparison, polishing the wrought Cu specimen yielded a smooth, featureless surface.

Figure 2 shows an SEM image of a polished cross section of the ADCS specimen. The sectioned specimen was etched with an  $NH_4OH$  solution to reveal the microstructure.<sup>25</sup> Figure 2(a) shows the individual surface depressions observed as flattened areas in Figure 1, and Figure 2(b) shows the presence of small pores,  $\sim 40 \text{ nm}$  to  $80 \text{ nm}$  in size, within the coating. Such a porosity was observed throughout the thickness of the coating. In addition to these nanocavities/pores, the Cu coating also contained sporadic larger cavities, some of which were up to  $40 \mu\text{m}$  to  $60 \mu\text{m}$  in width and extended significantly into the plane of the coating. Coatings formed with larger particles contained more pores, although generally, all coatings had a very low overall porosity ( $\ll 1\%$ ).<sup>24,26</sup> Although the focus of this study is not on optimization of coatings, it can be noted that higher particle velocity during fabrication decreases the coating porosity.<sup>27-28</sup> While annealing improves the crystallinity of the coating, as described elsewhere,<sup>26</sup> some of the nanopores remained (Figure 3). In addition, larger, coarse voids and pores were also observed (Figure 3[b]).

### Corrosion Under Anoxic Conditions

Figure 4 shows the evolution of  $E_{\text{corr}}$  on both the ADCS and WCu specimens. Over the first 7 d to 8 d,

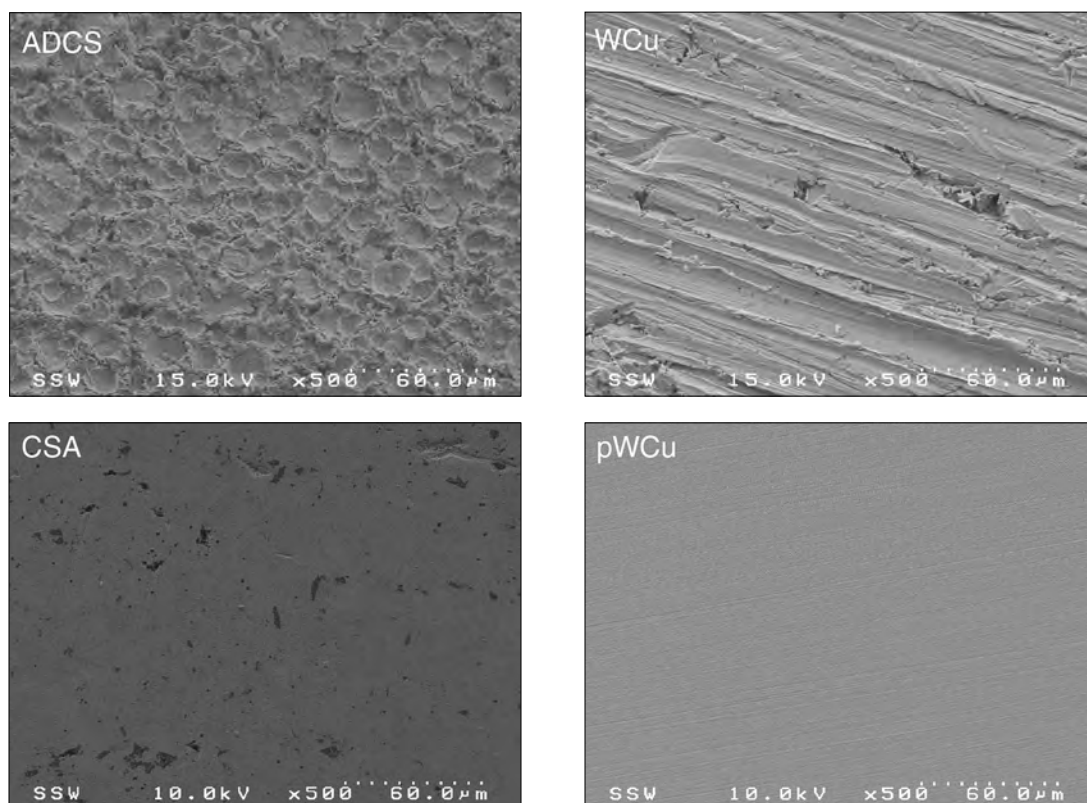


FIGURE 1. SEM images of the specimen surfaces prior to exposure to the 3.0 mol/L NaCl solution.

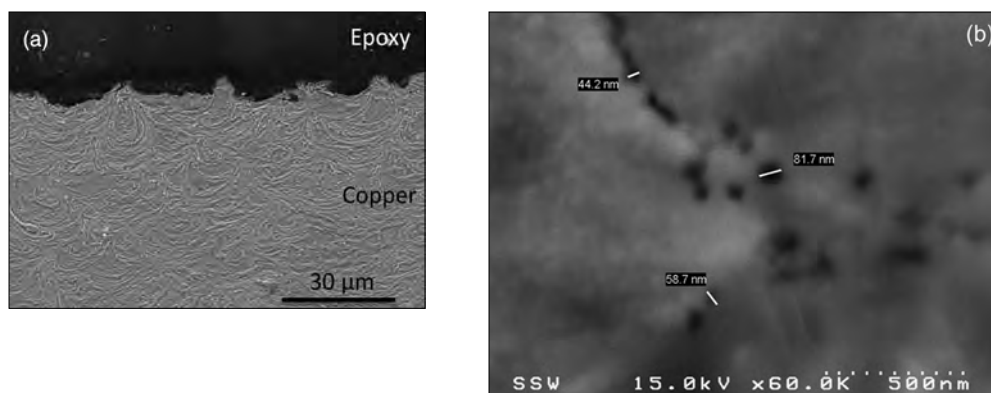
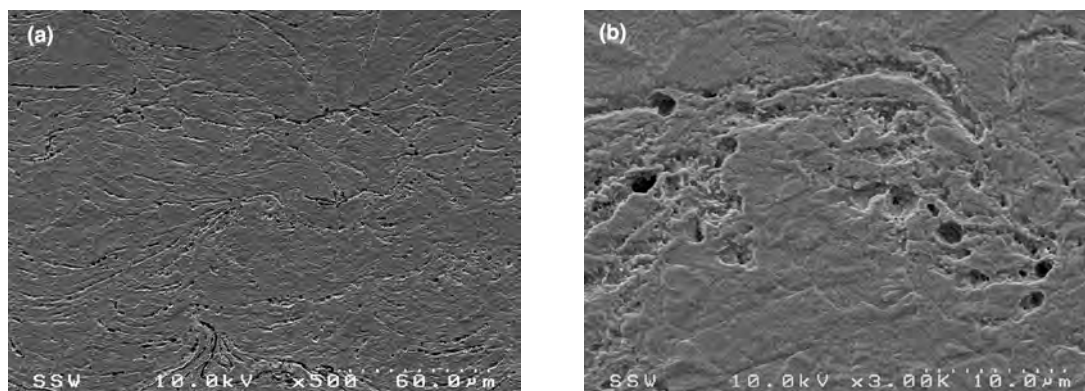


FIGURE 2. (a) SEM of the Cu coating on a polished and etched ADCS cross section and (b) nanopores within the Cu coating adjacent to the outer surface. The size distribution of the nanopores is indicated.

the  $E_{\text{corr}}$  values were very similar and in the range of  $-0.42 V_{\text{SCE}}$  to  $-0.43 V_{\text{SCE}}$ . These values are close to those measured and predicted for Cu in a deaerated 1 mol/L NaCl solution, as indicated by the line (A) in Figure 4.<sup>29-30</sup> The slightly more negative values would be expected in the more concentrated  $\text{Cl}^-$  solution used in these measurements. This comparison confirms the establishment of anoxic conditions. Over the longer exposure period, the values decreased and diverged slightly but followed close trajectories up to  $\sim 75$  d, beyond which  $E_{\text{corr}}$  for the WCu specimen decreased. No similar decrease in the  $E_{\text{corr}}$  was observed

on the ADCS specimen over this time period. The  $R_p$  values (Figure 5) for both specimens were effectively constant over the full exposure period. The  $R_p$  values, which were normalized to the geometric area, were close, suggesting the differences in active surface area between the two specimens (Figure 2) was not large. On both electrodes, the  $R_p$  values were in the range  $\sim 80 \text{ k}\Omega\cdot\text{cm}^2$  to  $150 \text{ k}\Omega\cdot\text{cm}^2$ . These values can be compared to the value estimated from electrochemical impedance measurements in pure  $\text{H}_2\text{O}$  ( $\sim 225 \text{ k}\Omega\cdot\text{cm}^2$ ) with a dissolved  $[\text{O}_2]$  estimated to be  $< 6.5 \text{ ppb}$ <sup>31</sup> (horizontal line (A) in Figure 5).



**FIGURE 3.** (a) SEM of the Cu coating on a polished and etched CSA cross section. (b) At a higher magnification nanopores can be seen to remain in the coating.

The  $O_2$  sensor in the anaerobic chamber showed that, over most of the experimental period, only minor excursions in the atmospheric  $O_2$  content of the chamber occurred, generally lasting  $\ll 1$  d. These excursions would be expected to exert a minimal influence on the dissolved  $[O_2]$  and appear undetected in the  $E_{\text{corr}}$  and  $R_p$  measurements. The slow decrease in  $E_{\text{corr}}$  up to  $\sim 72$  d may, therefore, reflect the slow consumption of residual dissolved  $O_2$  in the cell. Unfortunately, a failure of the chamber catalyst (used for controlling the generation of the anaerobic atmosphere within the chamber) allowed a short period of increased atmospheric  $O_2$  content over the final days of the exposure period. An increase in dissolved  $[O_2]$  would have led to an increase in  $E_{\text{corr}}$  (see Corrosion Under Oxygenated to Anaerobic Conditions section). However, the absence of any effect on  $R_p$  showed that this did not occur. On the ADCS specimen, the very slight decrease in  $R_p$  (i.e., increase in corrosion rate [proportional to  $R_p^{-1}$ ]) over this period can be attributed to corrosion of the steel substrate, which is a base material and its corrosion would be expected to occur at a more negative  $E_{\text{corr}}$ . Optical microscopy and EDX analyses confirmed the presence of Fe corrosion products at a number of locations where the epoxy resin had detached from the Cu.

Figure 6 shows the  $E_{\text{corr}}$  values recorded on the CSA and pWCu specimens. While initially establishing values approaching  $-0.4$   $V_{\text{SCE}}$ ,  $E_{\text{corr}}$  for both specimens rose rapidly (1 d to 2 d) to  $\sim -0.370$   $V_{\text{SCE}}$  and then changed only marginally over the subsequent  $\sim 125$  d exposure period. The  $R_p$  values are plotted in Figure 5 to facilitate their comparison to the values measured on the unpolished specimens. These values are initially up to a factor of 5 lower than those measured on the unpolished specimens but slowly increase to similar values over the subsequent 125 d exposure period. The values measured on the CSA and pWCu surfaces are very similar over the whole exposure period. The similarity in values for the unpolished and polished surfaces, at least for longer exposure periods,

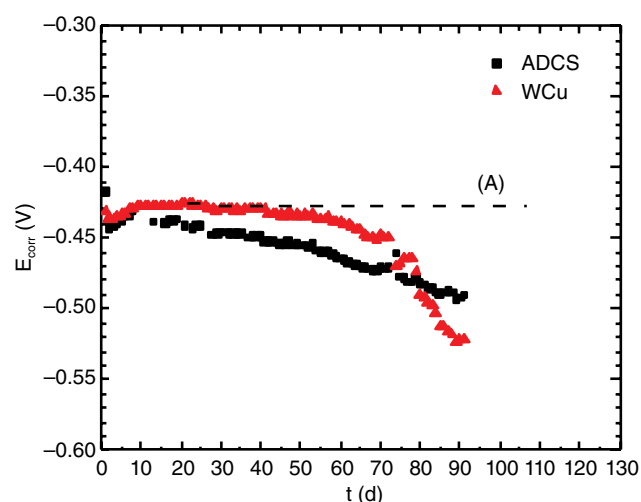


**FIGURE 4.** Evolution of  $E_{\text{corr}}$  with time for the WCu and ADCS specimens measured in 3.0 mol/L NaCl in an anaerobic chamber. The dashed line (A) shows the value measured in 1.0 mol/L NaCl.<sup>29</sup>

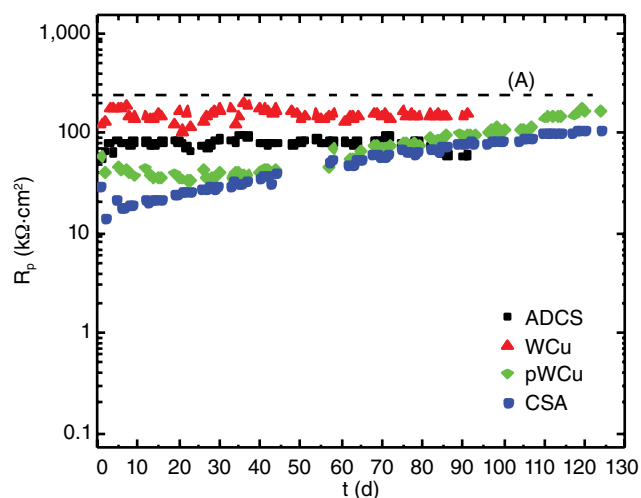


**FIGURE 5.** Evolution of the polarization resistance ( $R_p$ ) with time for WCu, ADCS, pWCu, and CSA specimens measured in 3.0 mol/L in an anaerobic chamber. The line (A) shows the value estimated from electrochemical impedance measurements in pure  $H_2O$ .<sup>31</sup>

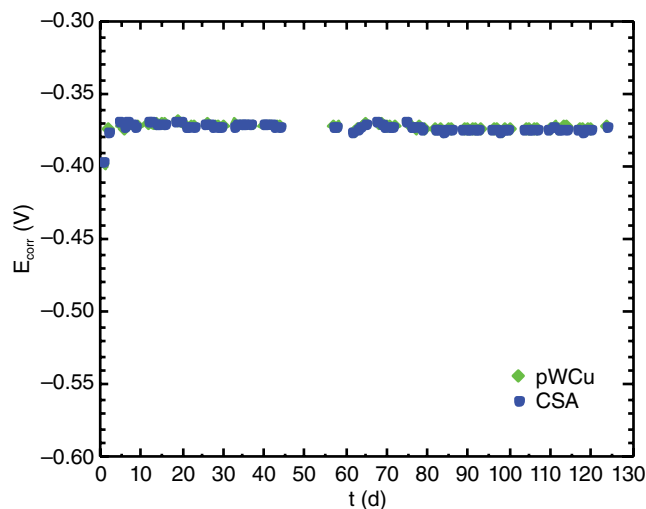


**FIGURE 6.** Evolution of  $E_{\text{corr}}$  values with time for the pWCu and CSA specimens measured in 3.0 mol/L NaCl in an anaerobic chamber.

suggests the active areas of all four specimens do not differ extensively.

### Corrosion Under Oxygenated to Anaerobic Conditions

Figures 7 and 8 show the evolution of  $E_{\text{corr}}$  and  $R_p$  for the ADCS and WCu specimens over a 24 d exposure to oxygenated conditions, followed by a 66 d exposure to Ar-sparged conditions. The  $E_{\text{corr}}$  values in the  $O_2$ -saturated solution were considerably more positive than observed under anoxic conditions. The dashed line (A) shows  $E_{\text{corr}}$  values measured and calculated in 1 mol/L NaCl.<sup>29-30</sup> As expected, the  $R_p$  values for both specimens (Figure 8) were considerably lower (one to two orders of magnitude) for these conditions when compared to the values measured under anaerobic conditions. Notably,  $E_{\text{corr}}$  for the ADCS specimen was slightly more positive than for the WCu specimen and showed some fluctuations. The sudden increase in  $E_{\text{corr}}$  (ADCS) after ~10 h (Figure 7) led to a decrease in  $R_p$  by a factor of 3 (Figure 8). This increase in corrosion rate (proportional to  $R_p^{-1}$ ) may indicate the detachment of corrosion products, as the electrode was suspended facing downward.

On switching to  $O_2$ -free conditions,  $E_{\text{corr}}$  rapidly decreased (over ~1 h) by ~0.120 V and then continued a more steady decrease on both specimens. Over the final 24 d of exposure, both specimens approached steady-state  $E_{\text{corr}}$  values, with the value for the WCu being ~40 mV more positive than the value for ADCS. The values were close to previous measurements made in 1 mol/L NaCl containing ~61 ppb of dissolved  $O_2$ ,<sup>29-30</sup> as indicated by line (B) in Figure 7. Over this same final 24 h period, the  $R_p$  values (Figure 8) also diverged slightly, with  $R_p$  (WCu) increasing slightly, while the value for the ADCS specimen remained almost constant. Two significant excursions

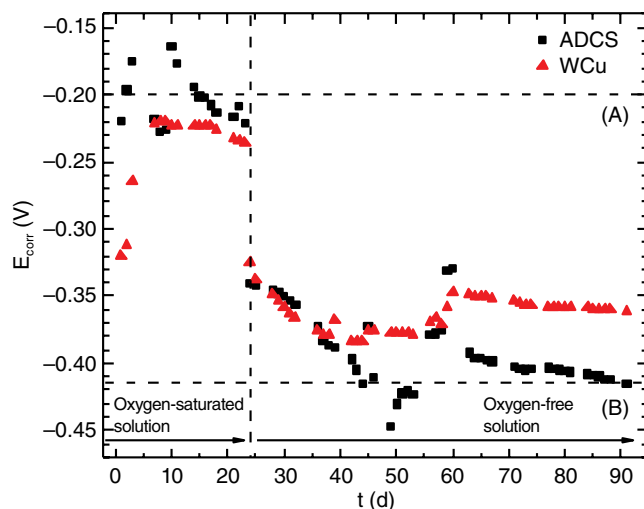


**FIGURE 7.** Evolution of  $E_{\text{corr}}$  with time for the ADCS and WCu specimens measured in an  $O_2$ -saturated 3.0 mol/L NaCl solution (up to 24 d), and in this solution sparged with Ar (beyond 24 d). Line (A) shows the value measured and calculated in 1.0 mol/L NaCl.<sup>29</sup> Line (B) shows the value measured in 1.0 mol/L NaCl containing ~61 ppb of dissolved  $O_2$ .<sup>29</sup>

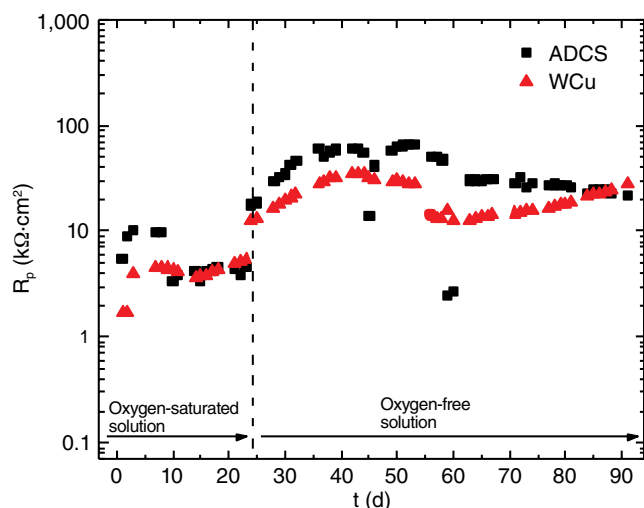


**FIGURE 8.** Evolution of polarization resistance ( $R_p$ ) with time for the ADCS and WCu specimens in an  $O_2$ -saturated solution (up to 24 d), and this solution sparged with Ar (beyond 24 d).

in  $E_{\text{corr}}$  (to more positive values leading to decreases in  $R_p$  [increases in corrosion rate]) were observed on the ADCS specimen at 45 d and 60 d. These excursions cannot be attributed to corrosion of the exposed steel substrate, for which a decrease in  $R_p$  would be accompanied by a decrease in  $E_{\text{corr}}$  (as discussed previously for anaerobic conditions). The most likely explanation is that these excursions reflect the detachment of corrosion products leading to the increased exposure of Cu and its corrosion by galvanic coupling to Cu(II)-containing corrosion product, with the reduction of Cu(II) leading to enhanced Cu corrosion to Cu(I) at the exposed location. A possible alternative explanation

would be a change in dissolved  $[O_2]$  resulting from a temporary loss of Ar-sparging. The fact that simultaneous excursions in  $R_p$  values were not observed on the WCu electrode may reflect protection of the surface of the latter as a result of a more comprehensive coverage by corrosion product deposits, although the slight decrease after  $\sim 53$  h could be attributed to a similar detachment of corrosion products. Even after 66 h of exposure to the Ar-sparged solution,  $E_{\text{corr}}$  for both specimens remained higher, and the  $R_p$  values lower, than the corresponding values achieved under anaerobic conditions.

Figures 9 and 10 show  $E_{\text{corr}}$  and  $R_p$  values measured in a similar oxygenated/Ar-sparged experiment conducted on the pWCu and CSA specimens. Under oxygenated conditions, the  $E_{\text{corr}}$  values were similar to those measured on the ADCS and WCu specimens, while the  $R_p$  values were considerably larger. The  $E_{\text{corr}}$  and  $R_p$  values for each specimen were plotted together to emphasize the matched variations, both showing simultaneous increases and decreases over the first 60 h exposure to oxygenated conditions. These variations can be attributed to periodic attempts to passivate by corrosion product deposition, followed by the detachment of the deposit and re-exposure of the bare Cu surface. This is demonstrated by the current-potential relationships recorded performing the LPR (not shown) that are distorted by the capacitance of the corrosion products at high values ( $> 100 \text{ k}\Omega\text{-cm}^2$ ) but not lower values. For this reason, the actual values of  $R_p$  recorded at positive  $E_{\text{corr}}$  are not particularly reliable.

On switching to Ar-sparged conditions (Figures 9 and 10),  $E_{\text{corr}}$  for both electrodes immediately fell to  $\sim -0.340 \text{ V}_{\text{SCE}}$  to  $-0.350 \text{ V}_{\text{SCE}}$ , and increased slightly over the subsequent 30 h before steadily decreasing to  $\sim -0.360 \text{ V}_{\text{SCE}}$  over the final 90 h of exposure. Despite the similarities in  $E_{\text{corr}}$ , the  $R_p$  values diverged over the 120 d period of Ar-sparging, with the value for WCu reaching  $\sim 100 \text{ k}\Omega\text{-cm}^2$ , close to the value achieved in anoxic conditions in the anaerobic chamber. By contrast, the  $R_p$  value for CSA hardly increased, remaining constant around  $\sim 30 \text{ k}\Omega\text{-cm}^2$ .

### Analysis of Corrosion Products

Optical images of the ADCS and WCu specimens are shown in Figure 11. After exposure in the anaerobic chamber, there was no visual evidence of corrosion on either specimen (Figures 11[a] and [c]). After exposure to the  $O_2/\text{Ar}$  environment, the ADCS specimen exhibited a reddish/brown color (Figure 11[b]), suggesting the presence of cuprite ( $\text{Cu}_2\text{O}$ ), while the WCu specimen appeared bright green (Figure 11[d]), indicative of the deposition of Cu(II) solids. Although not shown, both the CSA and pWCu specimens also showed no evidence of corrosion after exposure to anoxic conditions and were covered by a patchy green deposit after exposure to the  $O_2/\text{Ar}$  environment. The

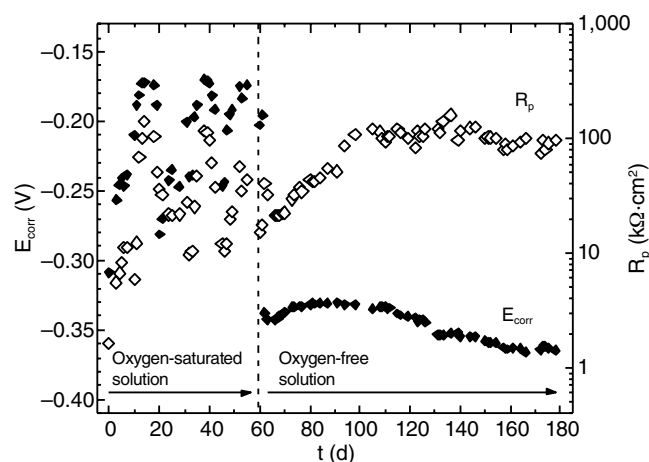


**FIGURE 9.** Evolution of  $E_{\text{corr}}$  (solid symbols) and  $R_p$  (hollow symbols) with time for the pWCu specimen in an  $O_2$ -saturated solution (up to 60 d), and this solution sparged with Ar (beyond 60 d).

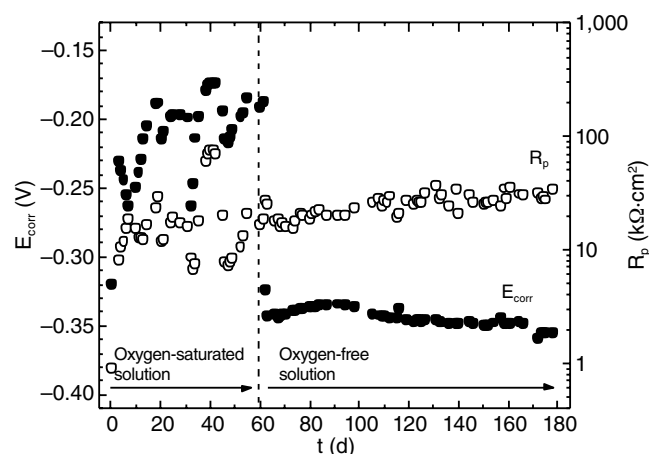


**FIGURE 10.** Evolution  $E_{\text{corr}}$  (solid symbols) and  $R_p$  (hollow symbols) with time for CSA samples in an oxygen-saturated solution (up to 60 d), and this solution sparged with Ar (beyond 60 d).

presence of this loosely adherent Cu(II) deposit was consistent with the periodicities observed in the  $E_{\text{corr}}$  and  $R_p$  measurements (Figures 9 and 10). The absence of corrosion on the ADCS and WCu specimens was confirmed by the SEM images in Figures 12(a) and (b), and Figures 12(c) and (d) confirmed the presence of corrosion products after exposure to  $O_2/\text{Ar}$  environments. Similar surface conditions were observed for the CSA and pWCu specimens (not shown).

XRD analyses of the ADCS and WCu specimens after anaerobic exposure did not detect any oxidized corrosion products but did demonstrate a difference in crystallographic orientation of the Cu, the (111) orientation being dominant for ADCS while the (220) orientation was dominant in the WCu. Additionally, the peaks in the ADCS pattern were broader than those in the WCu pattern, possibly reflecting the presence of considerable residual strain in the ADCS specimen.<sup>25</sup> Although not shown, analyses by x-ray photoelectron

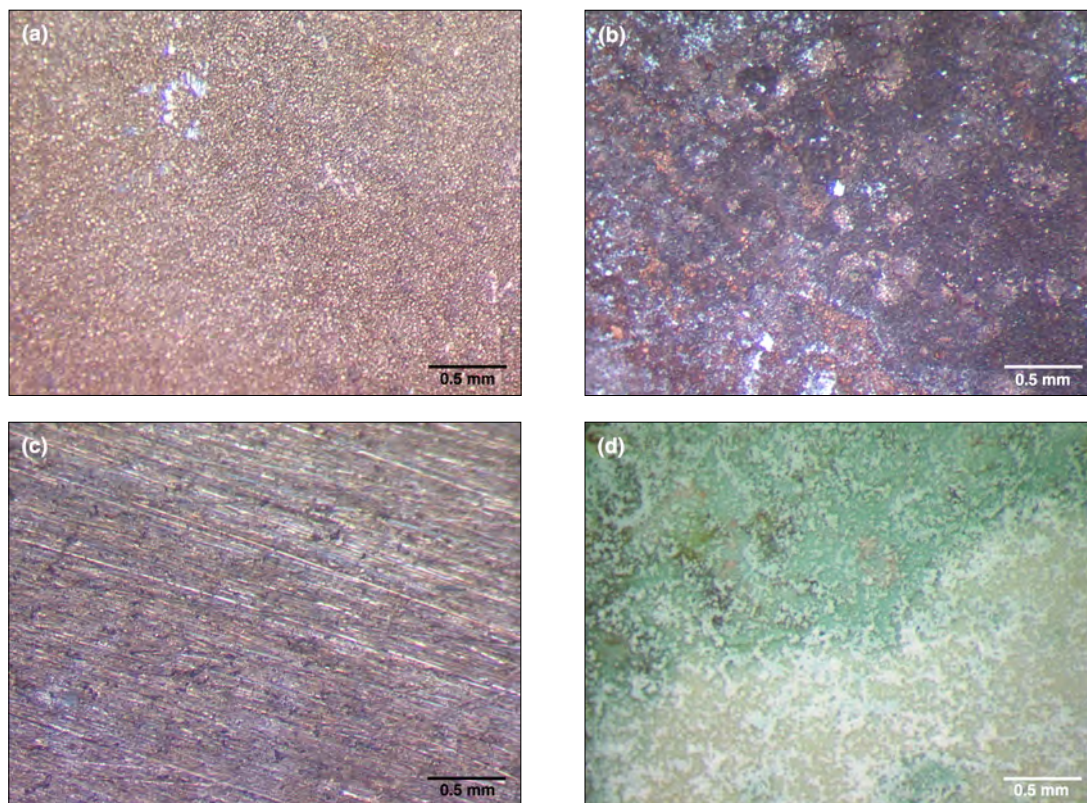


**FIGURE 11.** Optical microscopy images of the surface of the ADCS specimen after 90 d exposure to an O<sub>2</sub>-free (a) and an O<sub>2</sub>/Ar-sparged 3 mol/L NaCl solution (b). The corresponding images for the WCu specimen are presented in (c) and (d).

spectroscopy (XPS) detected only small amounts of Cu<sub>2</sub>O, most likely formed by air exposure on transfer of the specimens to the vacuum chamber of the spectrometer because any Cu<sub>2</sub>O formed during corrosion would dissolve in the concentrated chloride solution. For the ADCS specimen exposed to the O<sub>2</sub>/Ar environment, the only corrosion product detected was cuprite (Cu<sub>2</sub>O) (Figure 13[a]), consistent with the optical observation of a reddish/brown surface. For the WCu specimen, the dominant corrosion product was the cupric hydroxyl chloride (atacamite, Cu<sub>2</sub>(OH)<sub>3</sub>Cl), which would account for the green deposit and is consistent with previous observations<sup>31-34</sup> on Cu corrosion in aerated chloride solutions.

## DISCUSSION

The corrosion of Cu has been extensively studied in aerated chloride solutions<sup>29-30,32-35</sup> and, to a lesser degree, in anoxic aqueous solutions.<sup>31,36-38</sup> In many of these studies nominally under anoxic conditions, there was a good probability that residual traces of dissolved O<sub>2</sub> were present. Cleveland, et al., however, estimated the residual dissolved [O<sub>2</sub>] in their experiments to be < 6.5 ppb with the probability that it was as low as 1 ppb. Based on the extrapolation of EIS data to the zero frequency limit, they estimated the R<sub>p</sub> to be ~225 kΩ·cm<sup>2</sup>, which compares favorably with

this study's values of 80 kΩ·cm<sup>2</sup> to 200 kΩ·cm<sup>2</sup> obtained under anoxic conditions with a dissolved [O<sub>2</sub>] estimated to be < 1 ppb.

While Cleveland, et al., chose to convert their value to a corrosion rate using the Stern-Geary method, the authors of the present study have not done so for two reasons: (i) for some specimens, particularly ADCS and WCu, the area of the active Cu surface was uncertain, and (ii) it is likely that, at the scan rate applied in measuring the R<sub>p</sub> values using the LPR method, the value obtained would not be a truly direct current value. These caveats accepted, the R<sub>p</sub> values approached those estimated by Cleveland, et al., and, equally importantly, showed that there is little difference in corrosion behavior between the cold spray deposited Cu and commercially available wrought Cu.

Whether or not the corrosion of Cu to produce H<sub>2</sub> can occur under anoxic conditions has received considerable attention<sup>39-44</sup> and thermodynamic calculations indicate it is not inconceivable, provided the concentration of Cu<sup>+</sup> and the partial pressure of H<sub>2</sub> are sufficiently low.<sup>45</sup> Recent studies<sup>42-44</sup> show that sustained H<sub>2</sub> production is only observed with commercially produced Cu and can be avoided if the Cu is degassed by heating to 400°C (in vacuum), confirming that it is not produced by corrosion. The transitory formation of H<sub>2</sub> in a corrosion experiment could be

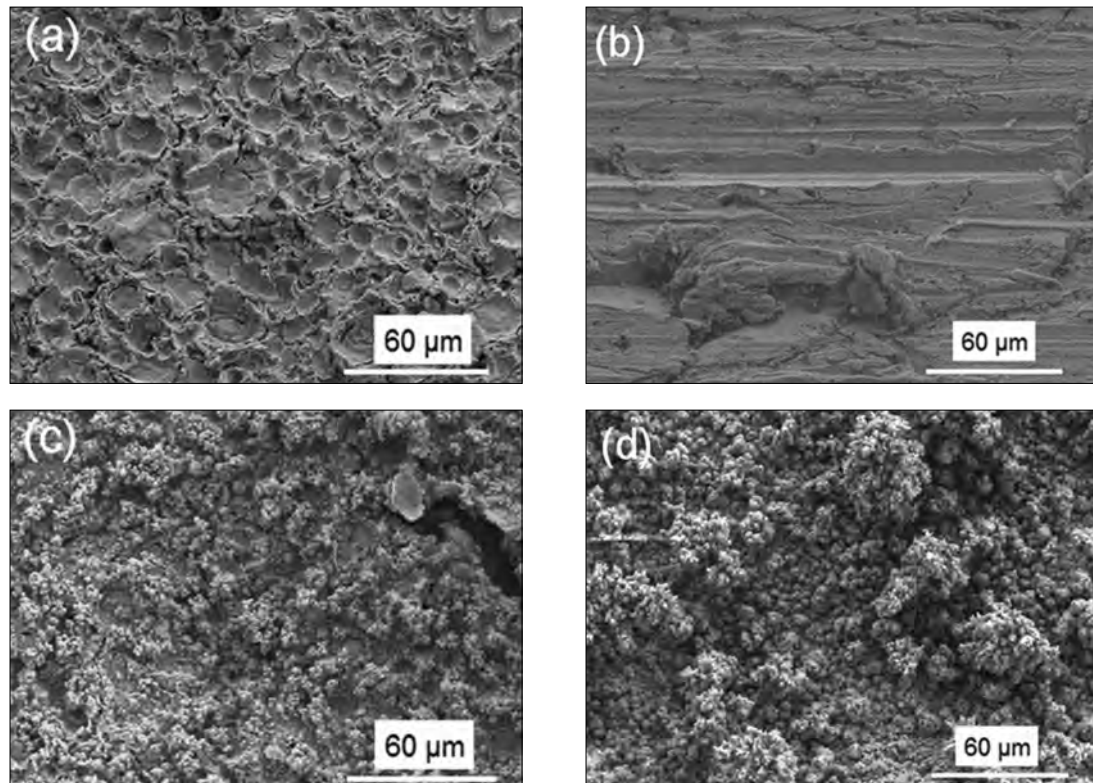


**FIGURE 12.** SEM micrographs of the surface of the ADCS specimen after exposure to  $O_2$ -free (a) and  $O_2/Ar$ -sparged 3 mol/L NaCl solution (c). The corresponding images for the WCu specimen are presented in (b) and (d).

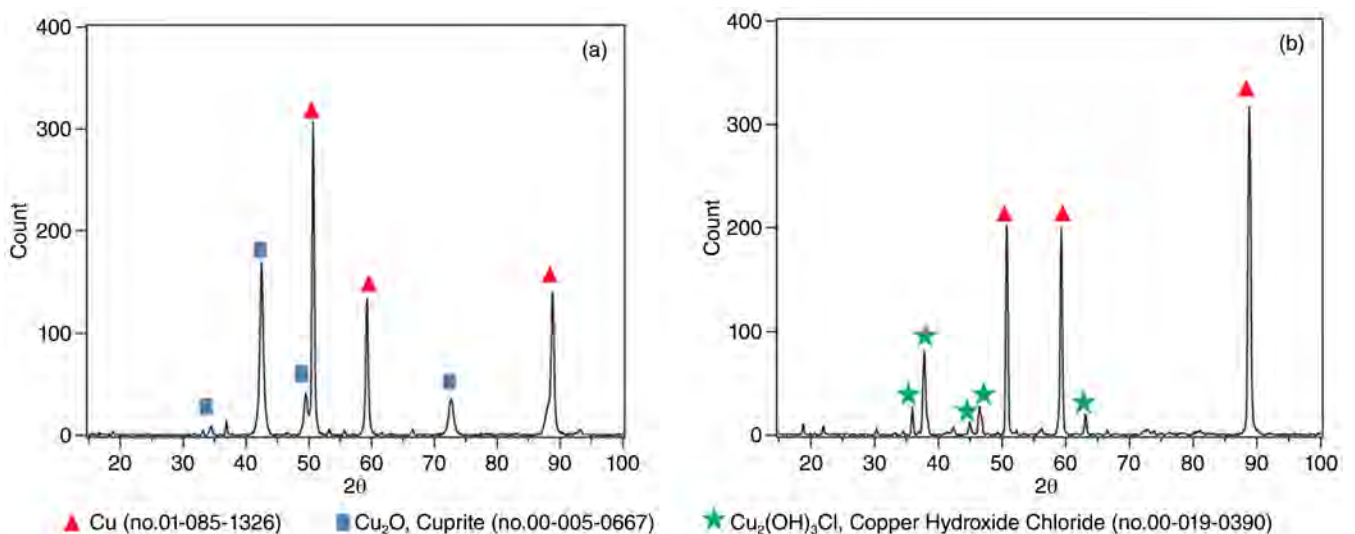


**FIGURE 13.** XRD patterns obtained for the ADCS (a) and WCu (b) samples after exposure to an  $O_2/Ar$ -sparged 3 mol/L NaCl solution. The peaks are identified by comparison with the PDF-card of the software used.

produced, however, on clean Cu scratched with SiC, suggesting a damaged (or cold worked) surface could undergo some anoxic corrosion to produce  $H_2$ . In the Swedish studies, this is a transitory effect.

These published studies suggest a number of possible reactions that could temporarily support Cu corrosion under anoxic conditions in this experiment:

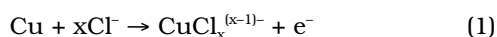
- i. A short period of reaction with  $H_2O$  resulting from the presence of a damaged surface;
- ii. The consumption of residual traces of dissolved  $O_2$  present despite efforts to remove it;
- iii. The presence of an air-formed Cu(II) oxide layer on first immersion of the specimen in the 3.0 mol/L NaCl solution.

A possibility is that the initially low, and slowly increasing, value of  $R_p$  observed on the two polished specimens (but not on the unpolished specimens) could be attributed to a period of anoxic corrosion producing  $H_2$  on the cold-worked surfaces that decreased to a negligible rate as the  $R_p$  value increased. This would introduce the possibility proposed by Cleveland, et al., that the  $H_2$  produced could itself eventually act as a reductant as equilibrium was approached. Because the experimental cell was open to the anaerobic chamber, the accumulation of dissolved  $H_2$  required for this to occur would be avoided, making the establishment of equilibrium conditions unlikely.

The consumption of residual traces of dissolved  $O_2$  would account for the initially lower  $R_p$  values, but would occur in experiments on both polished and unpolished specimens, and could not, therefore, account for the early differences in  $R_p$  values (Figure 5). However, the presence of an air-formed film, present on first immersion, would introduce the possibility of coupling of the Cu(II) oxide reduction to Cu metal dissolution to produce Cu(I), which would be soluble (as  $CuCl_x^{(x-1)-}$ ) in the concentrated  $Cl^-$  solution.

Bojinov, et al.,<sup>36</sup> have proposed that, in the presence of soluble  $Cu^{2+}$ ,  $H_2$  could be produced via a catalytic cycle involving the  $Cu^{2+}$  and a  $Cu(I)OH_{ads}$  surface intermediate. Because their experiments were performed in borate buffered solution, such a cycle may be feasible. However, in the 3 mol/L NaCl solution used in these experiments, this would be unlikely because the formation of  $CuCl_x^{(x-1)-}$  would be irreversible and the  $Cu^{2+}$  would eventually be consumed. This would limit the support of corrosion by any air-formed film to the inventory of Cu(II) present on the specimen surface on first immersion. It is possible that the oxide on the polished specimens is slightly thicker, and hence provides a bigger Cu(II) inventory than that on the unpolished specimens.

Under oxygenated conditions the general reaction in chloride solutions can be written:



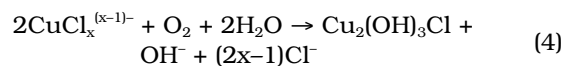
In the  $Cl^-$  solution, the anodic reaction is likely to proceed via a  $CuCl_{ads}$  surface intermediate which has a high solubility product<sup>45</sup> ( $1.72 \times 10^{-7}$ ) and will rapidly dissolve. Subsequently, consistent with this study's observations, deposition of corrosion products can proceed via one of two reactions:

(a) Hydrolysis to produce<sup>32</sup>  $Cu_2O$



(b) Homogeneous oxidation to produce<sup>47</sup>  $Cu^{2+}$  and the

deposition of Cu(II) solids, in particular atacamite<sup>48</sup>



According to King, et al.,<sup>30</sup> Cu(II) species can be reduced on the Cu surface and this reaction would be irreversible in concentrated  $Cl^-$  solution because of the formation of  $CuCl_x^{(x-1)-}$  soluble species. However, the analyses after the experiments involving an initial oxygenated period followed by Ar-sparging show copious deposits of atacamite persist, indicating this process is slow, on the time scale of these experiments, although it may be enhanced if areas of the Cu surface are exposed by detachment of the corrosion product. It is possible that this reaction could be accelerated in groundwater systems containing other anions<sup>30</sup> since  $Cu^{2+}$  solubility would be increased, a step that could accelerate the dissolution of Cu(II) deposits and facilitate their reaction with the Cu substrate to produce the soluble  $CuCl_x^{(x-1)-}$ . However, insufficient experimental evidence is available to confirm whether such an effect is observable.

## SUMMARY AND CONCLUSIONS

- ❖ The corrosion behavior of Cu cold spray coatings and commercially available wrought Cu are similar in 3 mol/L NaCl irrespective of the solution redox conditions. The corrosion potentials and polarization resistance values are consistent with the published literature for Cu corrosion.
- ❖ Under anoxic conditions (< 1 ppb dissolved  $O_2$ ), no corrosion was detectable over a 90 d to 120 d period, irrespective of whether the surface was polished or not. It is possible that extremely small amounts of corrosion, undetectable by the techniques used, could have occurred as a result of the presence of trace oxidants, of which the most likely are dissolved  $O_2$  and air-formed oxide films present on the specimen on first immersion. Whether or not the reaction of Cu with  $H_2O$  to produce  $H_2$  occurred could not be resolved by these studies.
- ❖ As expected from available literature, a combination of cuprite and atacamite is produced under oxygenated conditions. On subsequently switching to Ar-sparged conditions, these corrosion products appear to be stable. However, because the  $R_p$  values remain lower than under totally anoxic conditions, there is a possibility the Cu(II) corrosion products are being slowly consumed by reduction in a galvanic couple with Cu oxidation.
- ❖ There is no evidence that the particle boundaries between deposited cold spray particles are any more susceptible to corrosion under anoxic conditions than the general surface of the particles. After corrosion under oxidizing conditions, these boundaries are obscured beneath corrosion product deposits and more

detailed analyses are required to confirm whether or not corrosion is enhanced at these locations.

## ACKNOWLEDGMENTS

This research was funded by the Nuclear Waste Management Organization (NMWO), Toronto, Canada. National Research Council Canada (NRC) in Boucherville is thanked for the provided copper samples. The authors would like to thank Professor Roberta Fleming from the Geology Department at Western for her assistance with XRD measurements and Dr. Mark Biesinger for his assistance with the collection and interpretation of XPS data.

## REFERENCES

1. "Choosing a Way Forward: The Future Management of Canada's Used Nuclear Fuel," Nuclear Waste Management Organization, final summary, 2005, [http://www.nwmo.ca/uploads\\_managed/MediaFiles/342\\_NWMO\\_Final\\_Study\\_Summary\\_E.pdf](http://www.nwmo.ca/uploads_managed/MediaFiles/342_NWMO_Final_Study_Summary_E.pdf).
2. J. McMurry, D.A. Dixon, J.D. Garroni, B.M. Ikeda, S. Stroes-Gascoyne, P. Baumgartner, "Evolution of a Canadian Deep Geological Repository: Defective Container Scenario," Ontario Power Generation, Nuclear Waste Management Division, 06819-REP-01200-10092-R00, 2003.
3. F. King, "Status of the Understanding of Used Fuel Container Corrosion Processes—Summary of Current Knowledge and Gap Analysis," Nuclear Waste Management Organization, NWMO TR-2007-09, October 2007.
4. F. King, D.W. Shoesmith, "Nuclear Waste Canister Materials, Corrosion Behaviour and Long-Term Performance in Geological Repository Systems," in *Geological Repositories for Safe Disposal of Spent Nuclear Fuel and Radiation Materials*, eds. J. Ahn, M.J. Apted (Cambridge, UK: Woodhead Publishing Ltd, 2010).
5. P. Maak, G. Simmons, "Summary Report: A Screening Study of Used Fuel Container Geometries Designs and Emplacement Methods for a Deep Geologic Repository," Ontario Power Generation, Nuclear Waste Management Division, 06819-REP-01200-10005-R00, 2001.
6. P. Maak, *Materials Research Society Symposium Proceedings* 807 (2007): p. 447.
7. J.R. Scully, M. Edwards, "Review of the NWMO Copper Corrosion Allowance," Nuclear Waste Management Organization, NWMO TR-2013-04, May 2013.
8. W.H. Bowyer, "Design Basis for the Copper/Steel Canister," SKI, Report 98:29, June 1998.
9. C.G. Andersson, "Development of Fabrication Technology for Copper Canisters with Cast Inserts," SKB, SKB TR-02-07, April 2002.
10. W.H. Bowyer, "A Study of Defects Which Might Arise in the Copper Steel Canister," SKI, Report 00:19, May 1999.
11. M.S. Lee, H.J. Choi, J.W. Choi, H.J. Kim, *Nucl. Eng. Technol.* 43, 6 (2011): p. 557.
12. P.J. Henderson, J.-O. Österberg, B. Ivarsson, "Low Temperature Creep of Copper Intended for Nuclear Waste Containers," SKB, SKB TR 92-04, March 1992.
13. K. Pettersson, "A Review of the Creep Ductility of Copper for Nuclear Waste Canister Application," Stralsakerhetsmyndigheten, SSM Technical Note 2012:13, 2012.
14. C. Borchers, F. Gärtner, T. Stoltenhoff, H. Assadi, H. Kreye, *J. Appl. Phys.* 93, 12 (2003): p. 10064.
15. H.J. Choi, M. Lee, J.Y. Lee, *Nucl. Eng. Design* 240, 10 (2010): p. 2714.
16. T. Stoltenhoff, H. Kreye, H.J. Richter, *J. Thermal Spray Technol.* 11, 4 (2002): p. 542.
17. ASTM B152, "Standard Specification for Copper Sheet, Strip, Plate, and Rolled Bar" (West Conshohocken, PA: ASTM, 2013).
18. H.C. Macan, "Protecting Electrodeposited Metal Surfaces," U.S. Patent 2324859, 1940.
19. ASTM D1193-06, "Standard Specification for Reagent Water" (West Conshohocken, PA: ASTM, 2011).
20. R. Sander, *Atmospheric Chemistry and Physics*, 15 (2015): p. 4399.
21. H. Koivuluoto, J. Lagerbom, M. Kylmälahti, P. Vuoristo, *J. Thermal Spray Technol.* 17, 5-6 (2008): p. 721.
22. H. Koivuluoto, J. Lagerbom, P. Vuoristo, *J. Thermal Spray Technol.* 16, 4 (2007): p. 488.
23. T. Kaireit, M. Degrez, F. Campana, J.P. Janssen, *J. Thermal Spray Technol.* 16, 5-6 (2007): p. 610.
24. V. Phuong, D. Poirier, E. Irissou, J.G. Legoux, "Cold Sprayed Corrosion Protection Coating for Nuclear Waste Repository Canister," report submitted to Nuclear Waste Management, National Research Council Canada, 2012.
25. R.N. Caron, R.G. Barth, D.E. Tyler, "Metallography and Microstructures of Copper and Its Alloys," in *Metallography and Microstructures*, ASM Handbook vol. 9, ed. G.F. Vander Voort, (Materials Park, OH: ASM International, 2004), p. 775-788.
26. P. Jakupi, P.G. Keech, I. Barker, S. Ramamurthy, R.L. Jacklin, D.W. Shoesmith, D.E. Moser, *J. Nucl. Mater.* 466 (2015): p. 1-11.
27. S.H. Zahiri, D. Fraser, S. Gulizia, M. Jahedi, *J. Thermal Spray Technol.* 15, 3 (2006): p. 422.
28. P.C. King, S.H. Zahiri, M. Jahedi, *Metall. Mater. Trans. A* 40, 9 (2009): p. 2115.
29. F. King, C.D. Litke, M.J. Quinn, D.M. Leneveu, *Corros. Sci.* 37, 5 (1995): p. 833.
30. F. King, C. Lilja, K. Pederson, P. Pitkanen, M. Vahanen, "An Update of the State-of-the-Art Report on the Corrosion of Copper Under Expected Conditions in a Deep Geologic Repository," Swedish Nuclear Fuel and Waste Management, TR-10-67, December 2010.
31. C. Cleveland, S. Moghaddam, M.E. Orazem, *J. Electrochem. Soc.* 161, 3 (2014): p. C107.
32. G. Kear, B.D. Barker, F.C. Walsh, *Corros. Sci.* 46, 1 (2004): p. 109.
33. C. Deslouis, B. Tribollet, G. Mengoli, M.M. Musiani, *J. Appl. Electrochem.* 18, 3 (1988): p. 374.
34. T. Kosec, Z. Qin, J. Chen, A. Legat, D.W. Shoesmith, *Corros. Sci.* 90 (2015): p. 248.
35. F. King, L. Ahonen, C. Taxén, U. Vuorinen, L. Werme, "Copper Corrosion Under Expected Conditions in a Deep Geologic Repository," Swedish Nuclear Fuel and Waste Management, TR-01-23, 2001.
36. M. Bojinov, I. Betova, C. Lilja, *Corros. Sci.* 52, 9 (2010): p. 2917.
37. R. Dortwegt, E. Maugham, "The Chemistry of Copper in Water and Related Studies at the Advanced Photon Source," Particle Accelerator Conference (New York, NY: IEEE, 2001), p. 1456-1458.
38. R. Dortwegt, C. Putman, E. Swetin, "Mitigation of Copper Corrosion and Agglomeration in APS Process Water Systems," 2nd International Workshop on Mechanical Engineering Design of Synchrotron Radiation Equipment and Instrumentation (MEDSI02) (Argonne, IL: Argonne National Laboratory, 2002), p. 462-468.
39. G. Hultquist, P. Szakalos, M.J. Graham, A.B. Belonoshko, G.I. Sproule, L. Grasjo, P. Dorogokupets, B. Danilov, T. Aastrup, G. Wikmark, G.K. Chuah, J.C. Eriksson, A. Rosengren, *Catalysis Letters* 132, 3-4 (2009): p. 311.
40. G. Hultquist, M.J. Graham, P. Szakalos, G.I. Sproule, A. Rosengren, L. Grasjo, *Corros. Sci.* 53, 1 (2011): p. 310.
41. P. Szakalos, G. Hultquist, G. Wikmark, *Electrochem. Solid State Letters* 10, 11 (2007): p. C63.
42. A. Bengtsson, A. Chukarkina, L. Eriksson, B. Hallbeck, L. Hallbeck, J. Johansson, L. Johansson, K. Pedersen, "Development of Method for the Study of H<sub>2</sub> Gas Emission in Sealed Compartments Containing Canister Copper Immersed in O<sub>2</sub>-Free Water," Swedish Nuclear Fuel and Waste Management Co., Technical Report TR-13-13, June 2013.
43. M. Boman, M. Ottoson, R. Berger, Y. Andersson, M. Hahlin, F. Bjorefors, T. Gustafsson, "Corrosion of Copper in Ultra-Pure Water," Swedish Nuclear Fuel and Waste Management Co., SKB R-14-07, April 2014.
44. A. Hedin, C. Lilja, J. Johansson, "Copper corrosion in oxygen free water – Status report," Swedish Nuclear Fuel and Waste Management Co., 2014.
45. D.D. Macdonald, S. Sharifi-Asl, "Is Copper Immune to Corrosion When in Contact With Water and Aqueous Solutions?," Swedish Radiation Safety Authority, SSM Technical Note 2011:09, 2011.
46. D.R. Lide, *Handbook of Chemistry and Physics*, 86th ed. (Boca Raton, FL: Taylor and Francis, 2005).
47. V.K. Sharma, F.J. Millero, *J. Solution Chemistry* 17, 6 (1988): p. 581.
48. H.P. Lee, K. Nobe, *J. Electrochem. Soc.* 133, 10 (1986): p. 2035.